Electronic Supplementary Information

$K_{1.5}VOPO_4F_{0.5}$: A Novel High-Power and High-Voltage Cathode for Rechargeable K-Ion Batteries

Hyunyoung Park[a], *Wonseok Ko*[a], *Yongseok Lee*[a], *Jungmin Kang*[a], *Jinho Ahn*[a], *Jung-Keun Yoo*[*b] *and Jongsoon Kim*[*a]

[a]Department of Energy Science, Sungkyunkwan University, Suwon, 16419, Republic of Korea

[b]Carbon Composites Department, Composites Research Division, Korea Institute of Materials Science (KIMS), 797 Changwondaero, Changwon, Republic of Korea

Corresponding Authors: Dr. Jung-Keun Yoo (yoojk@kims.re.kr) and Prof. Jongsoon Kim (jongsoonkim@skku.edu).

Supplementary discussion

S1. Further synthesis attempts of $K_xVOPO_4F_{0.5}$ through wet-chemical methods

Further experiments for synthesize $K_{1.5}VOPO_4F_{0.5}$ were conducted through sol-gel synthesis and hydrothermal synthesis. We used the various precursors stoichiometrically, such as NH_4VO_3 (99%, Alfa Aesar), KF (99%, Sigma Aldrich), K_2CO_3 (99%, Daejung chemical) and $NH_4H_2PO_4$ (98.5%, Sigma Aldrich). The detailed sol-gel synthesis and hydrothermal synthesis processes are as follow;

(1) For the sol-gel synthesis, the four precursor powders were dissolved in 1 mol L^{-1} citric acid solution, and stirred at 80 ℃ for 6 h. The homogeneous solution was dried in oven at 120 ℃ for overnight, then after dried gel was grounded and heated at 600 ℃ for 6 h under an Ar atmosphere.

(2) For the hydrothermal synthesis, the four precursor powders were dissolved in distilled water, and stirred at 90 ℃ for 30 min. Then after, the solution was heated using polytetrafluoroethylene (PTFE) lined steel autoclave vessel at 180 ℃ for 24 h.

As shown in **Fig. S1a**, however, it was verified through the XRD measurement that only amorphous phases, not $K_xVOPO_4F_{0.5}$ phase are just formed after the sol-gel synthesis method. In case of the hydrothermal synthesis method, any powders were formed after the synthesis process (**Fig. S1b**). These results indicate that it is very difficult to synthesize $K_xVOPO_4F_{0.5}$ phase via the wet-chemical synthesis methods such as sol-gel synthesis and hydrothermal synthesis.

S2. Reversible K^+/Na^+ ion-exchange in $K_{1.5}VOPO_4F_{0.5}$

To verify the re-obtained $Na_{1.5}VOPO_4F_{0.5}$ phase from $K_{1.5}VOPO_4F_{0.5}$, the $K_{1.5}VOPO_4F_{0.5}$ electrode was assembled into a Na-ion cell with 0.5 M $NaPF_6$ in propylene carbonate (PC):fluoroethylene carbonate (FEC) (volume ratio of 98:2) electrolyte. And then, the we performed 30 times charge/discharge process of Na metal//0.5 M $NaPF_6$ in PC:FEC//$K_{1.5}VOPO_4F_{0.5}$ cell at the current rate of 1C (1C = 130 mA g^{-1}) (**Fig. S2a**). After the repeated cycling, we performed *ex-situ* XRD analyses on the cycled $K_{1.5}VOPO_4F_{0.5}$ electrode under the NIB system. As shown in **Fig. S2b**, it was verified that crystal structure of re-obtained $Na_{1.5}VOPO_4F_{0.5}$ phase from $K_{1.5}VOPO_4F_{0.5}$ is highly similar with that of pristine $Na_{1.5}VOPO_4F_{0.5}$. Furthermore, through the ICP analyses (**Table S1**), it was demonstrated that all K^+ in $K_{1.5}VOPO_4F_{0.5}$ are exchanged to Na^+ after the repeated cycling under the NIB system.

S3. Determining the cut-off voltage of $K_{1.5}VOPO_4F_{0.5}$ ion-exchange process

In this study, a cut-off voltage of 4.5 V was selected for deintercalating more Na ions from $Na_{1.5}VOPO_4F_{0.5}$ structure efficiently. As shown in **Fig. S3a**, we performed the several Na^+/K^+ ion-exchange processes from $Na_{1.5}VOPO_4F_{0.5}$ to $K_{1.5}VOPO_4F_{0.5}$ with changing charge cut-off voltage from 4.3 V to 4.5 V. It was verified that specific capacities after charging to 4.5 V are larger than those after charging to 4.3 and 4.4 V, which implies that more Na^+/K^+ ion-exchange is occurred at charge cut-off voltage of 4.5 V than those of 4.3 and 4.4 V. Moreover, **Fig. S3b** presents that the crystal structures of the samples are similar with each other despite different charge cut-off voltage, indicating well retention of the crystal structure during Na^+/K^+ ion-exchange process. However, some difference among the XRD patterns of each sample is also observed, such as difference of intensity ratio among (002), (111), (113), (220), (004) and (222) peaks, which indicates that degree of ion-exchange from Na^+ to K^+ at each sample are different from each other. As tabulated in **Table S2**, in particular, ICP results indicate that all Na ions are exchanged to K ions during 30 cycles with charge cut-off voltages of 4.5 V whereas partial Na ions still exist at the structure after 30 cycles with charge cut-off voltages of not only 4.3 V but also 4.4 V.

S4. The Na^+ storage performance of $Na_{1.5}VOPO_4F_{0.5}$

The electrochemical properties of $Na_{1.5}VOPO_4F_{0.5}$ was verified in the NIB system using Na metal as the counter electrode and 0.5 M $NaPF_6$ in propylene carbonate (PC):fluoroethylene carbonate (FEC) (volume ratio of 98:2) as the electrolyte. As shown in **Fig. S4**, $Na_{1.5}VOPO_4F_{0.5}$ delivered specific capacity of ~130 mAh g^{-1} measured at C/20 (1C = 130 mA g^{-1}) in the voltage range of 1.8–4.4 V, corresponding to de/intercalation of ~1 mol Na^+ in the structure. Even at 5C, the specific capacity of $Na_{1.5}VOPO_4F_{0.5}$ at 5C was reached ~86% of the capacity measured at C/20. In the cycle test, $Na_{1.5}VOPO_4F_{0.5}$ retained ~95% of its initial capacity after 100 cycles measured at 1C with Coulombic efficiency of more than ~99%.

S5. Detailed properties of heat-treated hard carbon anode

To verify the effect of heat-treatment, XRD and XPS analyses were performed on hard carbon before and after heat-treatment of 1000 ℃. As shown in **Fig. S5**, there are none of significant change with XRD patterns between pristine hard carbon and heat-treated hard carbon, which means the hard carbon structure is maintained during the heat-treatment process. On the other hand, it was verified that the peak intensities of O-H (530.6 eV) and H_2O (533.8 eV) bonds are reduced after heat-treatment, indicating the removal of residual moisture and organic impurities in hard carbon through the heat-treatment (**Fig. S6**).[1–4] The electrochemical properties of hard carbon anode are highly affected by existence and nonexistence of heat-treatment. As shown in **Fig. S7**, whereas pristine hard carbon anode exhibits just ~207 mAh g^{-1} at the current rate of 10 mA g^{-1}, the hard carbon anode after heat-treatment delivers ~298 mAh g^{-1} at the same conditions. Furthermore, the specific capacity of the heat-treated hard carbon anode after 100 cycles is maintained up to ~89 % compared to its initial capacity. In case of the pristine hard carbon anode, however, it just delivers ~76 % capacity retention for 100 cycles, which is poor compared to the cycle-performance of the heat-treated hard carbon anode (**Fig. S8**). These results indicate that heat-treatment of hard carbon is essential to improve the overall electrochemical performance.

Supplementary figure

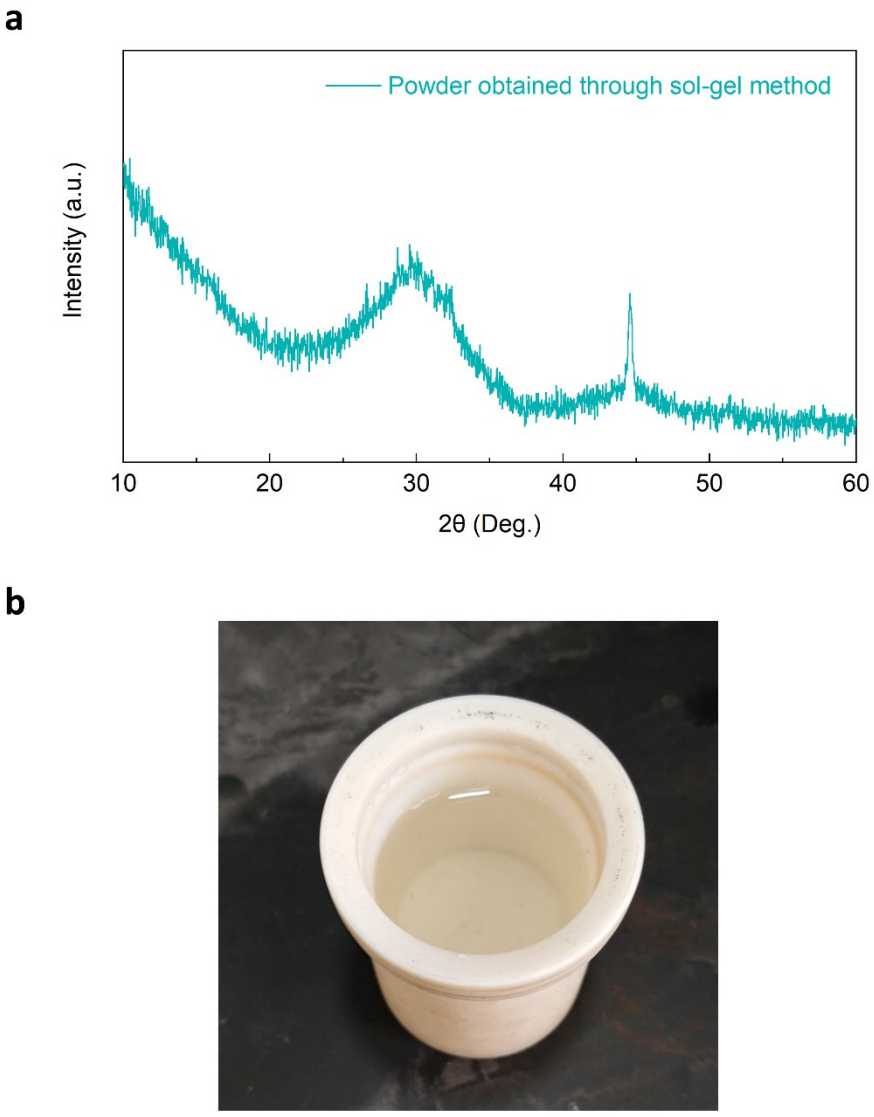

Fig. S1 (a) XRD pattern of powder obtained through sol-gel method. (b) Precursor solution after hydrothermal treatment.

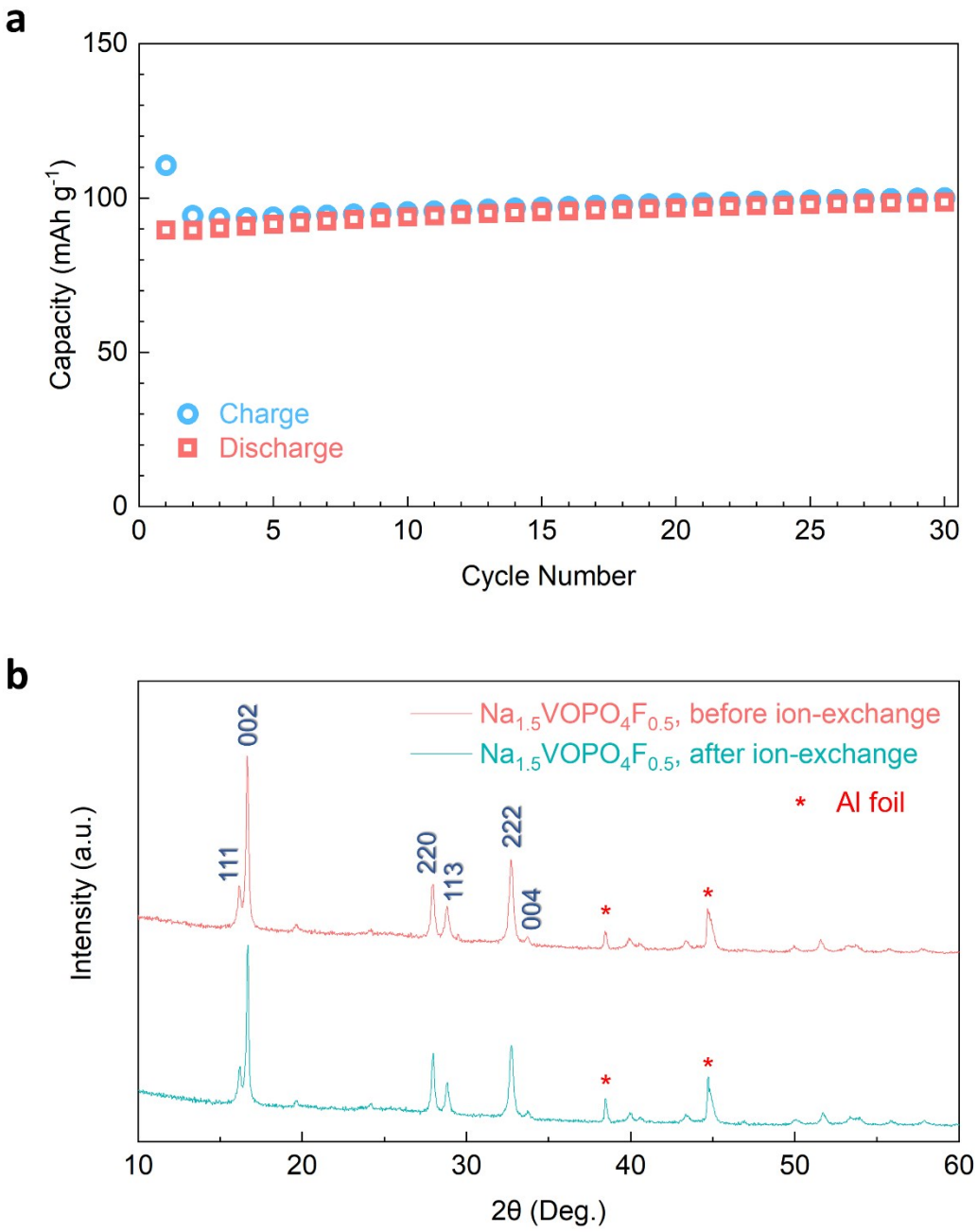

Fig. S2 (a) Electrochemical ion-exchange process of Na metal//0.5 M $NaPF_6$ in PC:FEC (volume ratio of 98:2)//$K_{1.5}VOPO_4F_{0.5}$ half-cell. (b) XRD pattern of $Na_xVOPO_4F_{0.5}$ after the K^+/Na^+ ion-exchange process.

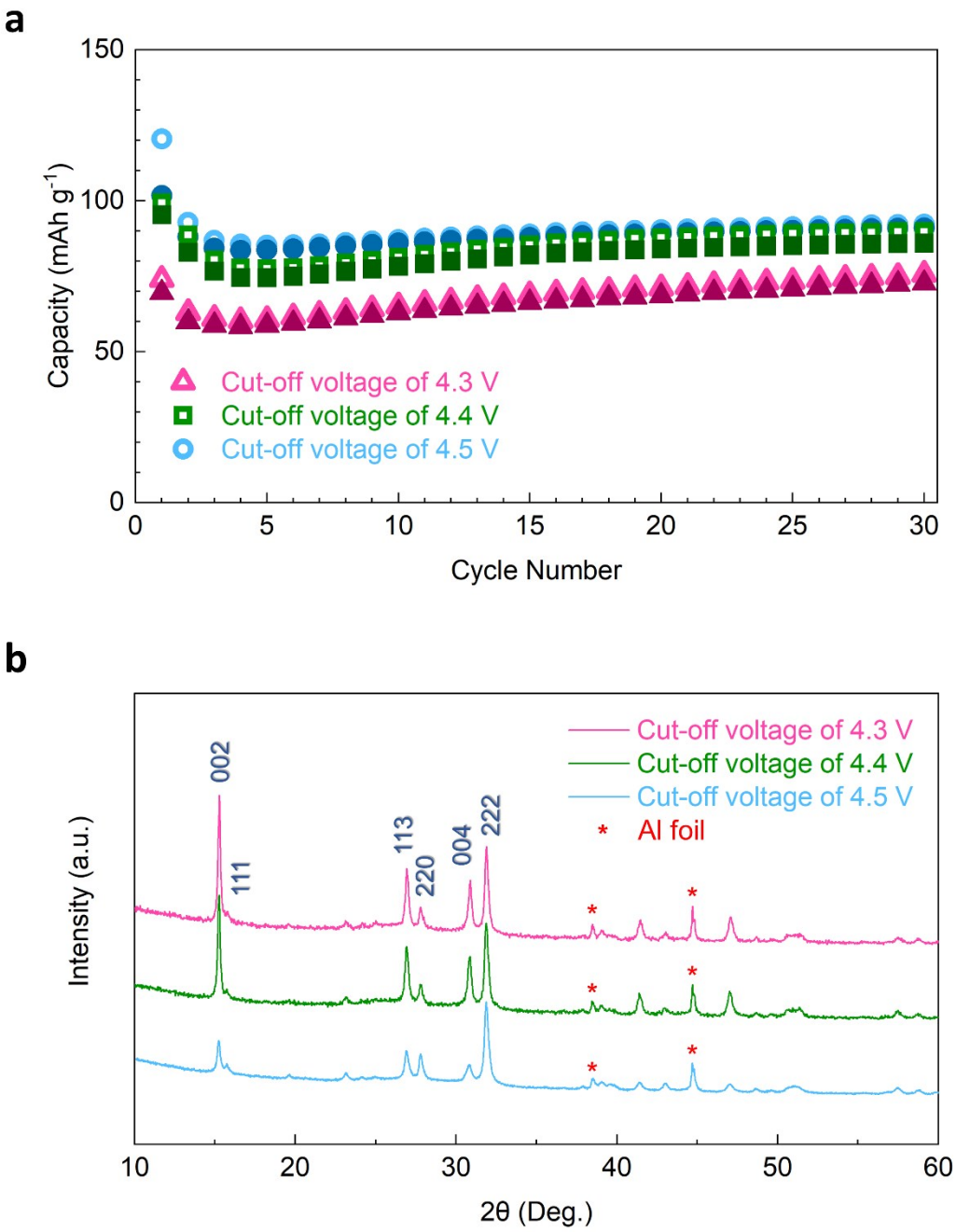

Fig. S3 (a) Electrochemical ion-exchange process of K metal//0.5 M KPF_6 in EC:PC (volume ratio of 1:1)//$K_{1.5}VOPO_4F_{0.5}$ half-cell with different cut-off voltage. (b) XRD patterns of $K_{1.5}VOPO_4F_{0.5}$ with different cut-off voltage.

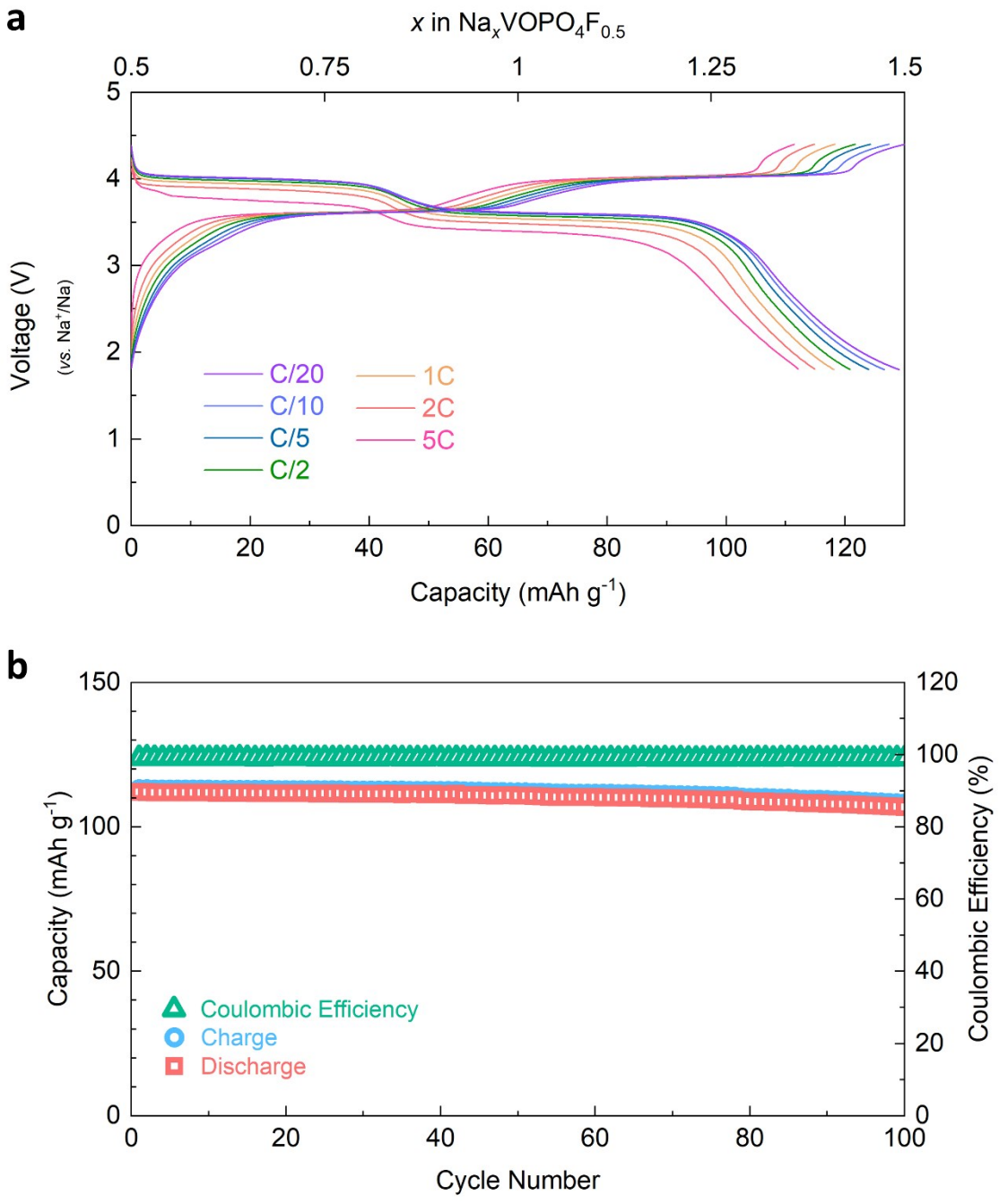

Fig. S4 (a) Charge/discharge curves of $Na_{1.5}VOPO_4F_{0.5}$ in the voltage range of 1.8–4.4 V at various discharge current rates (1C = 130 mA g^{-1}). (b) Cycling performance of $Na_{1.5}VOPO_4F_{0.5}$ over 100 cycles at 1C.

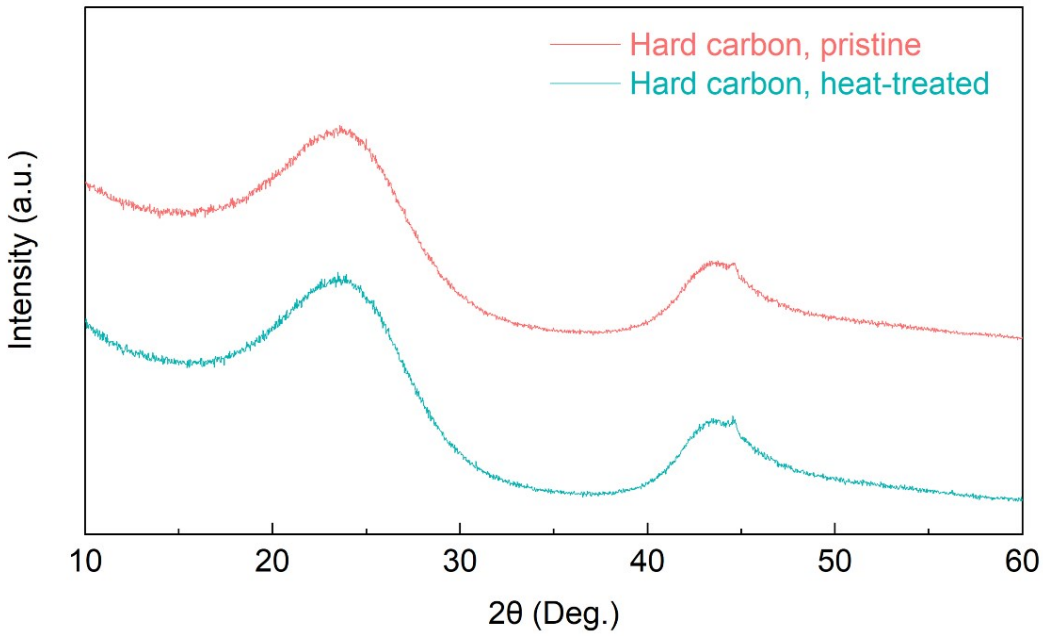

Fig. S5 XRD patterns comparison between pristine and heat-treated hard carbon.

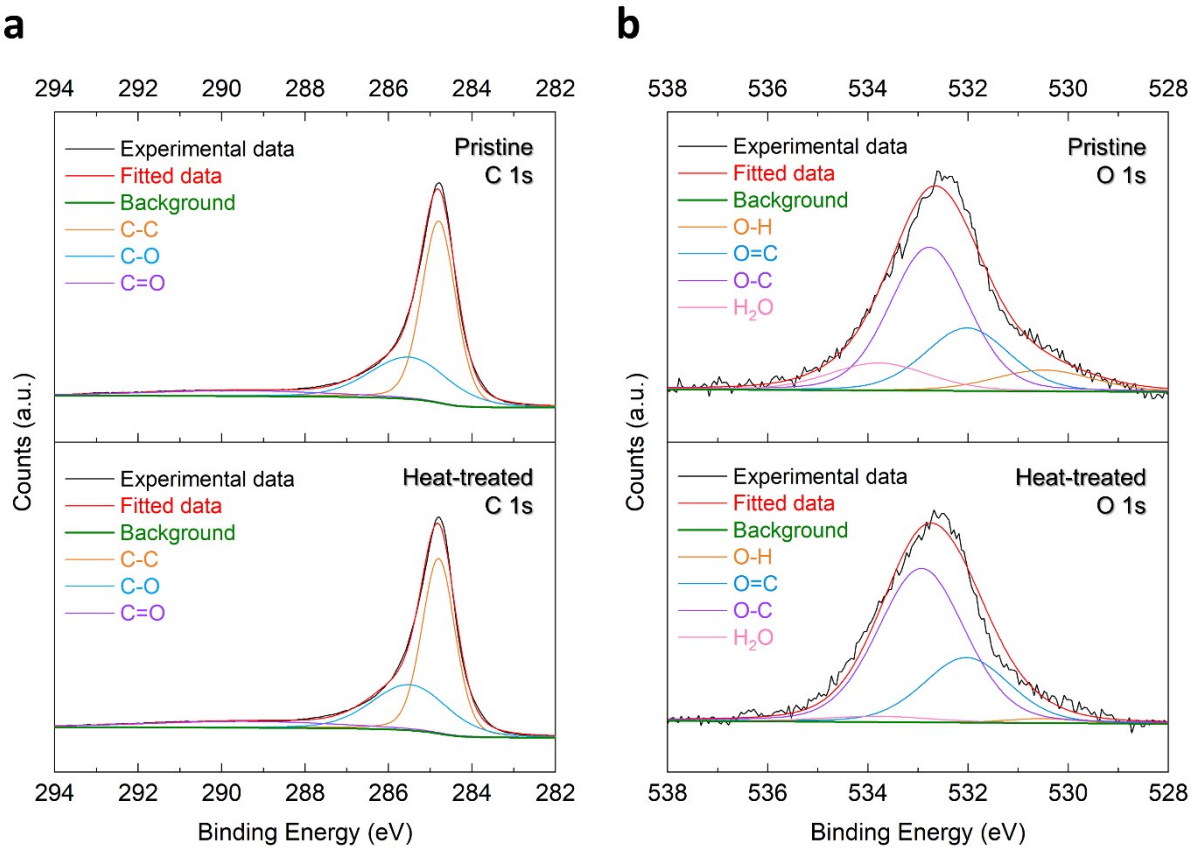

Fig. S6 (a and b) XPS spectra comparison between pristine and heat-treated hard carbon for (a) C 1s and (b) O 1s.

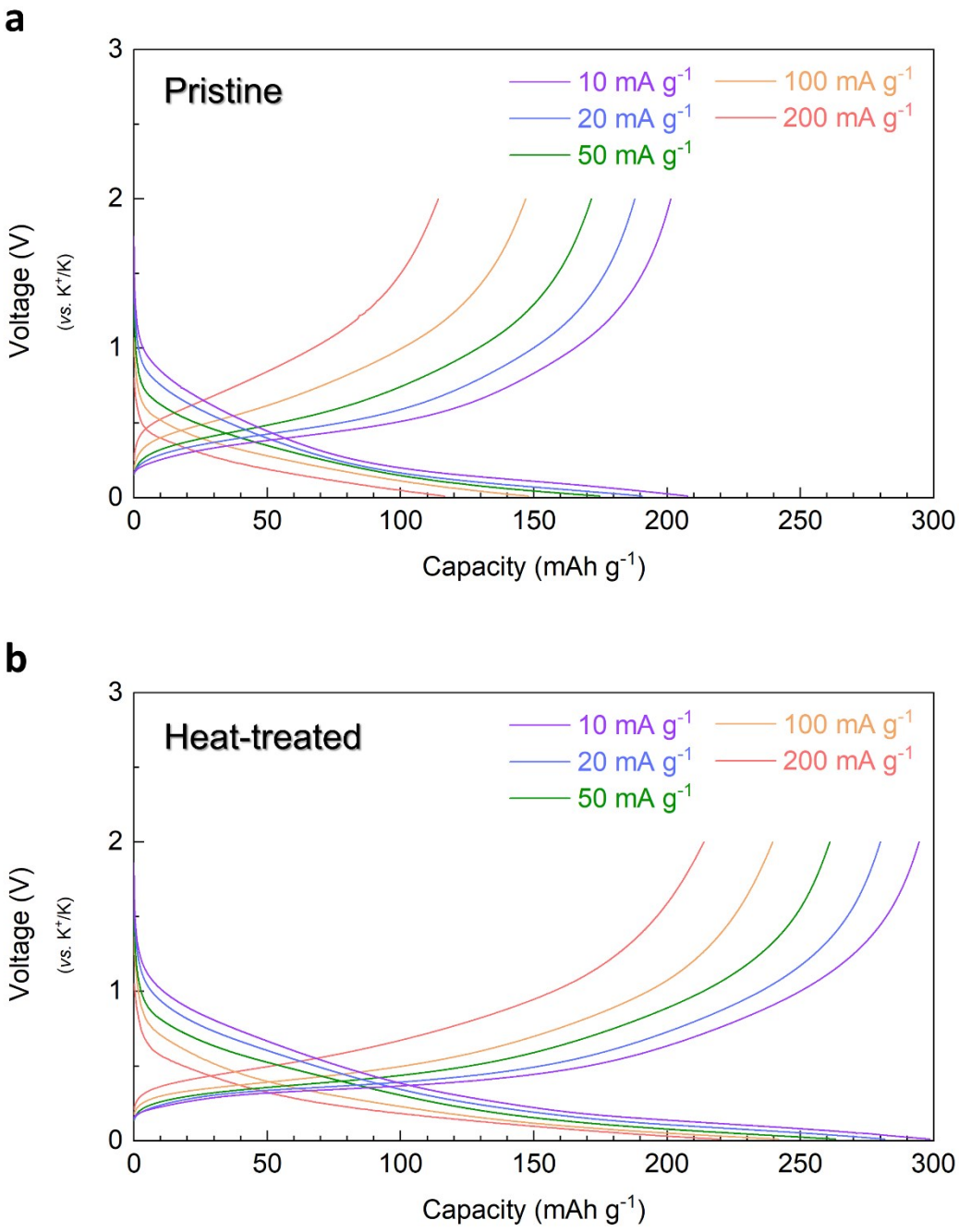

Fig. S7 (a and b) Charge/discharge curves of (a) pristine hard carbon and (b) heat-treated hard carbon in the voltage range of 0.01–2.0 V at various discharge current rates.

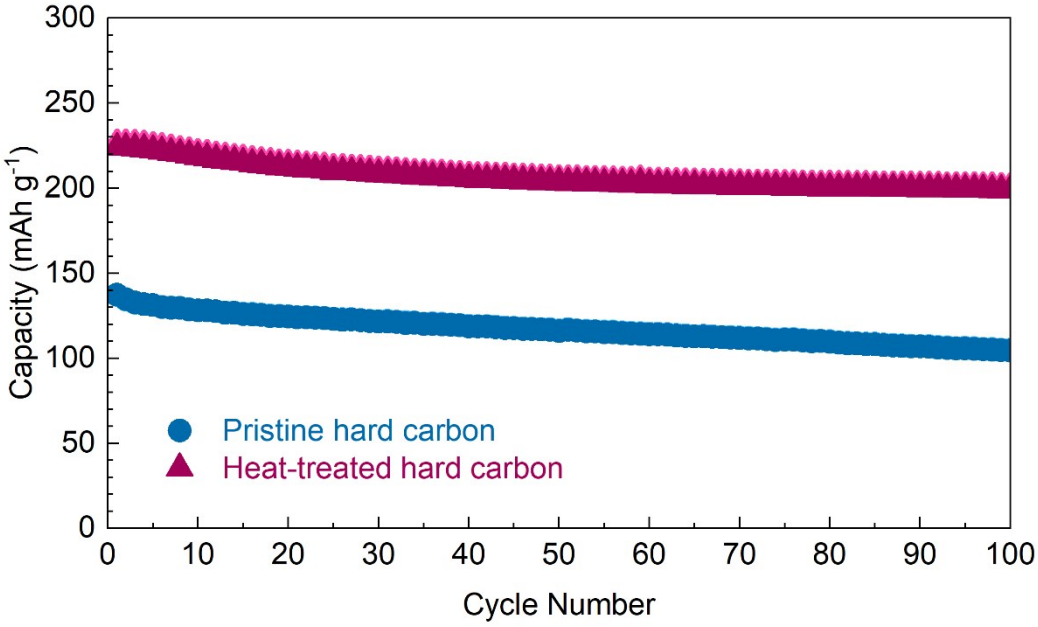

Fig. S8 Cycling performance of hard carbon over 100 cycles at 100 mA g^{-1}.

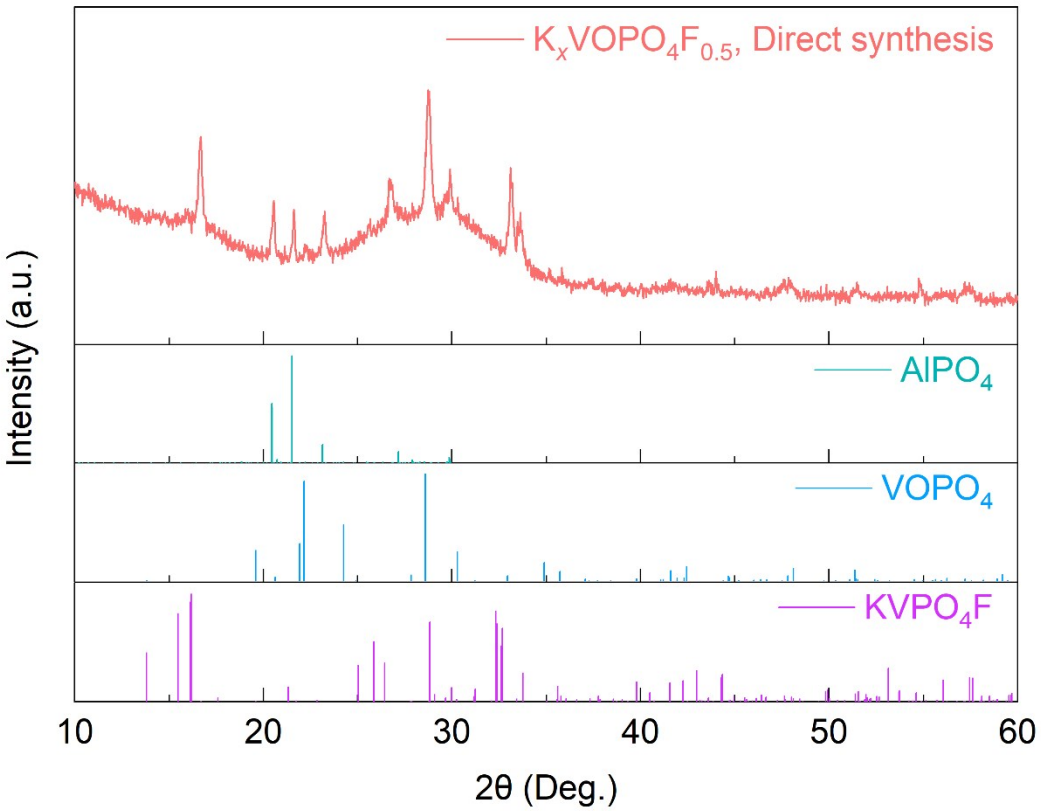

Fig. S9 XRD pattern of $K_xVOPO_4F_{0.5}$ via direct synthesis. Noted that Al element was originated from the alumina crucible.

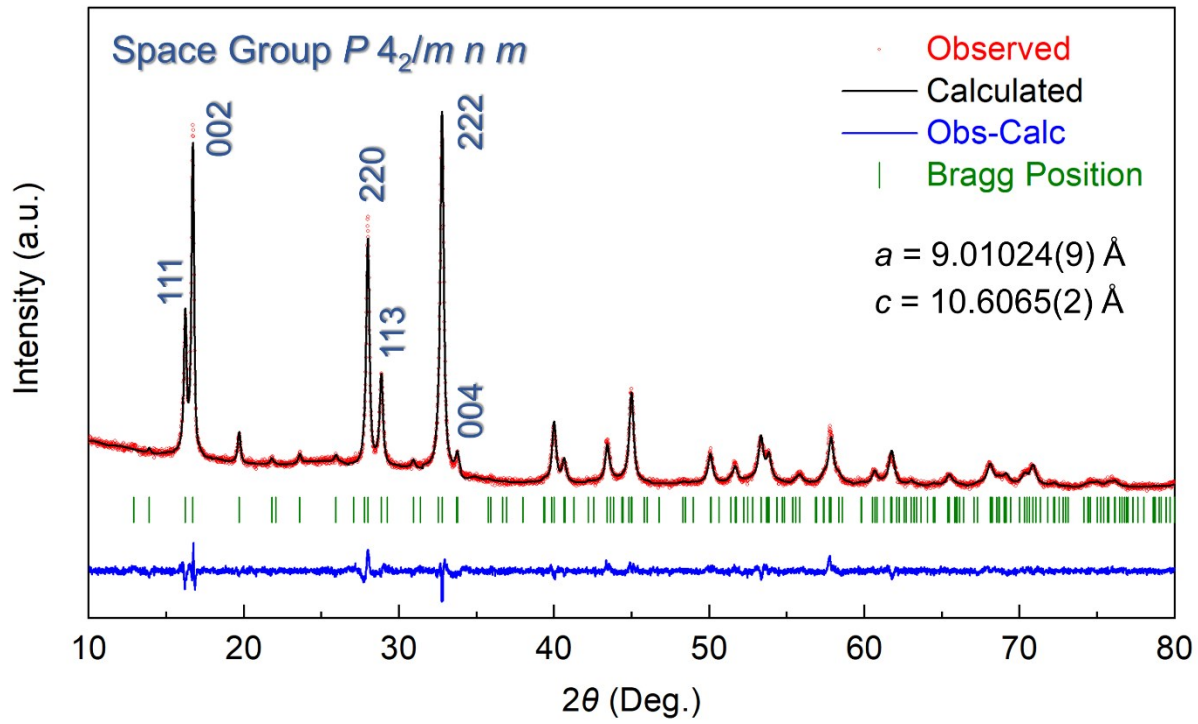

Fig. S10 Refined XRD pattern of $Na_{1.5}VOPO_4F$ using Rietveld refinement (R_p = 2.50%, R_{wp} = 3.19%, R_I = 4.24%, R_F = 3.28%, and χ^2 = 1.78%).

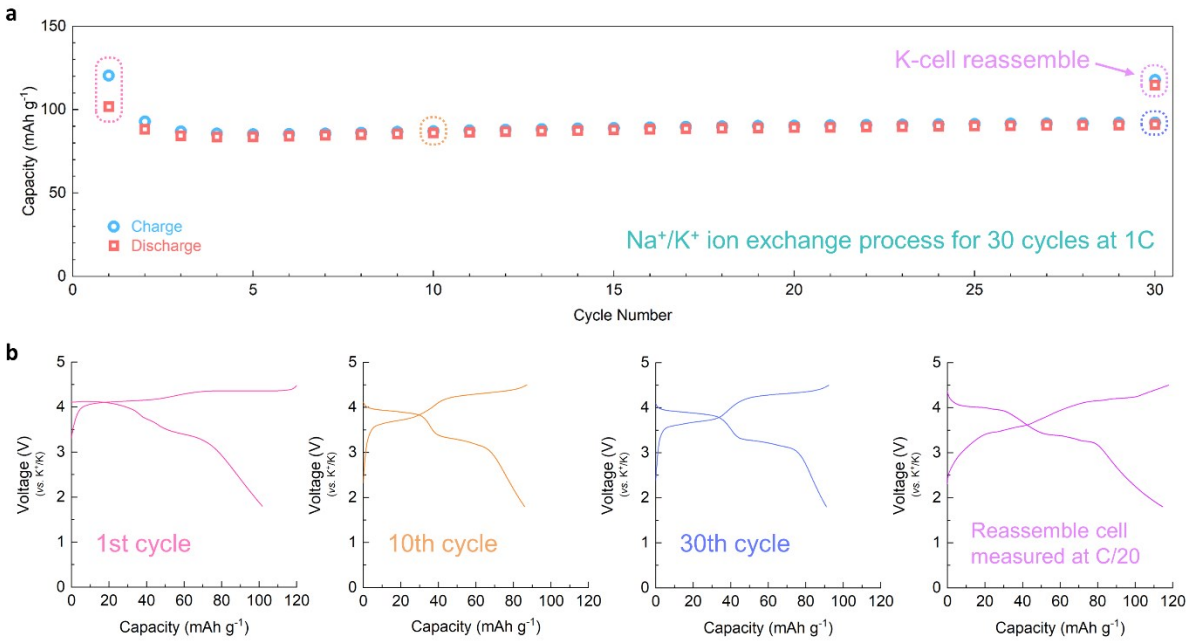

Fig. S11 (a) Electrochemical ion-exchange process of K metal//0.5 M KPF_6 in EC:PC (volume ratio of 1:1)//$Na_{1.5}VOPO_4F_{0.5}$ half-cell. (b) Charge/discharge profiles of K metal//0.5 M KPF_6 in EC:PC (volume ratio of 1:1)//$Na_{1.5}VOPO_4F_{0.5}$ half-cell.

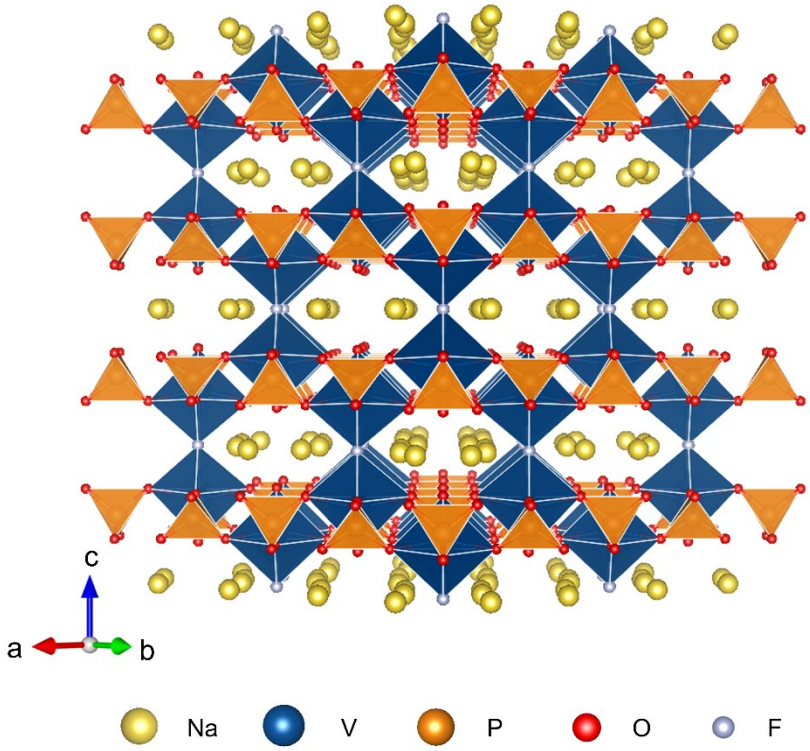

Fig. S12 Crystal structure of $Na_{1.5}VOPO_4F_{0.5}$. The crystal structure of $Na_{1.5}VOPO_4F_{0.5}$ structure is composed of corner-sharing between $[V_2O_{10}F]$ bi-octahedra and $[PO_4]$ tetrahedra, which provides the stable 3-dimensional framework and large atomic sites for storage of alkali-ions such as Na^+. The structural information of $Na_{1.5}VOPO_4F_{0.5}$ also indicate that stable 3-dimensional open framework of $Na_{1.5}VOPO_4F_{0.5}$ can be stably retained even after ion-exchange from Na^+ to K^+ and numerous K^+ can be stored at the structure.

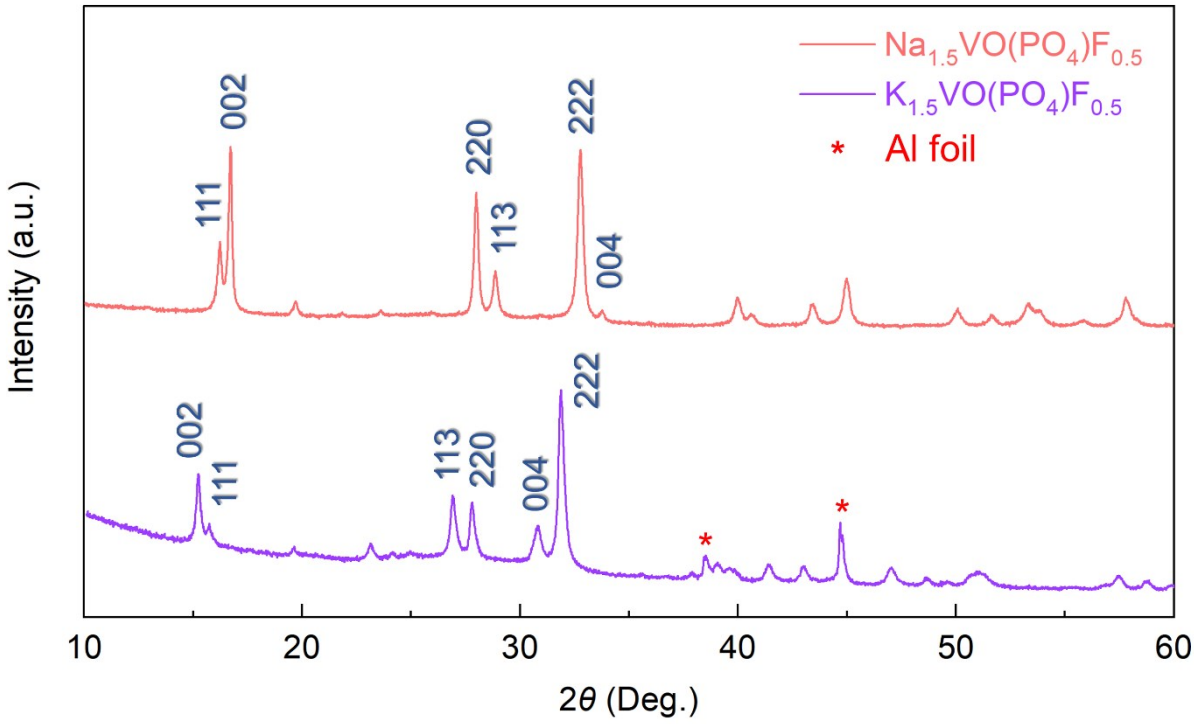

Fig. S13 XRD pattern comparison between $Na_{1.5}VOPO_4F_{0.5}$ and $K_{1.5}VOPO_4F_{0.5}$.

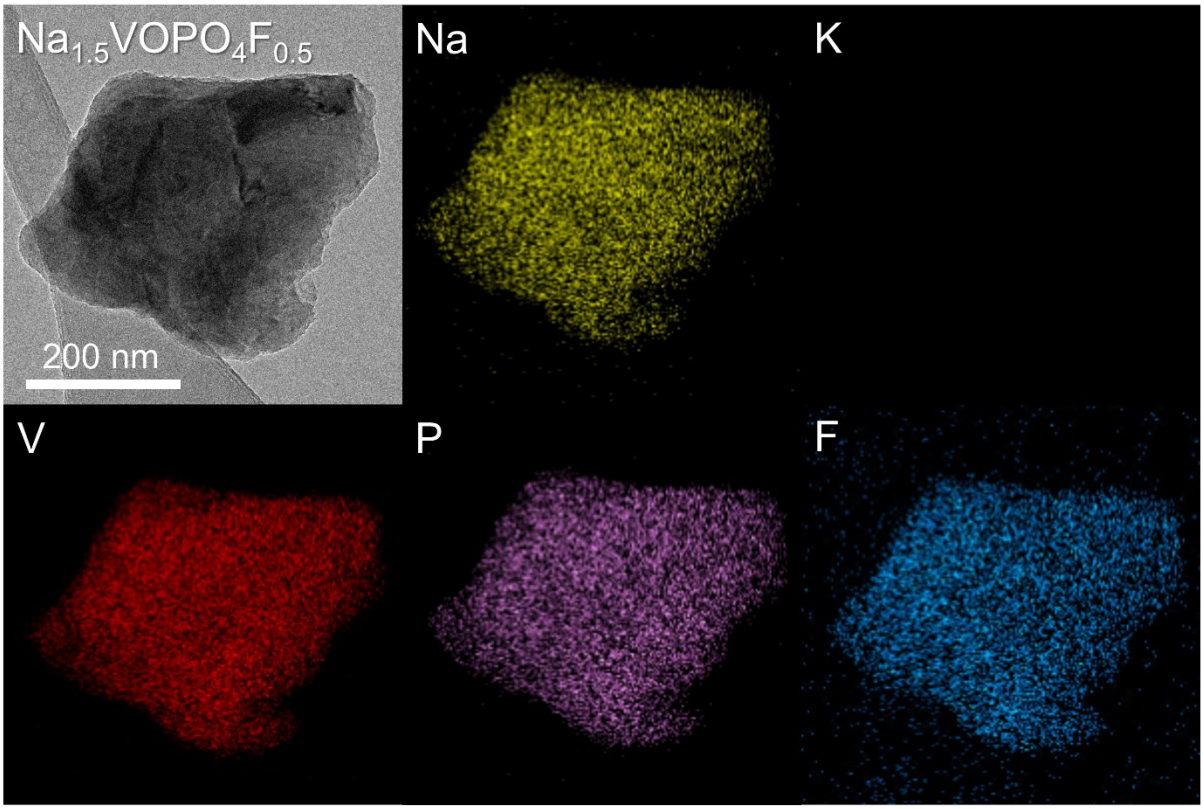

Fig. S14 TEM-EDS analyses of $Na_{1.5}VOPO_4F_{0.5}$.

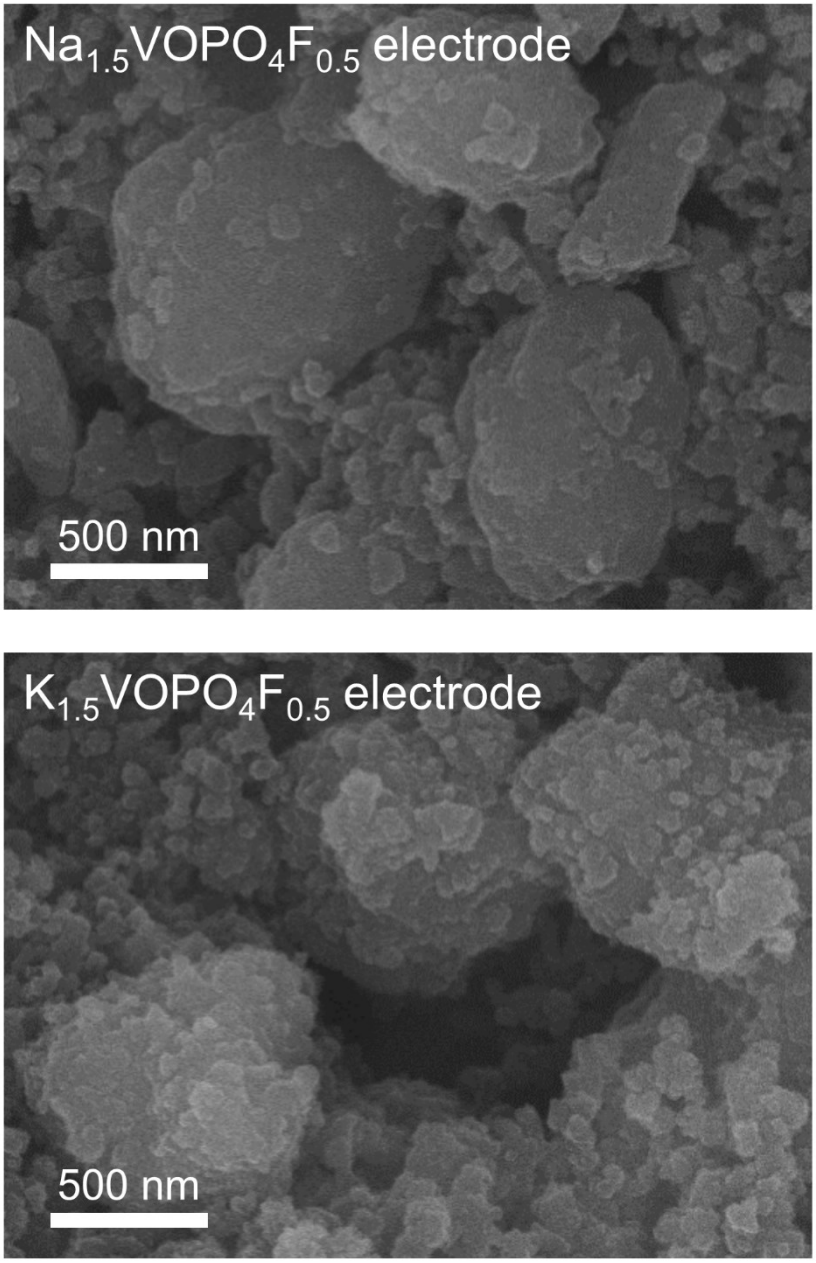

Fig. S15 SEM analyses of $Na_{1.5}VOPO_4F_{0.5}$ and $K_{1.5}VOPO_4F_{0.5}$

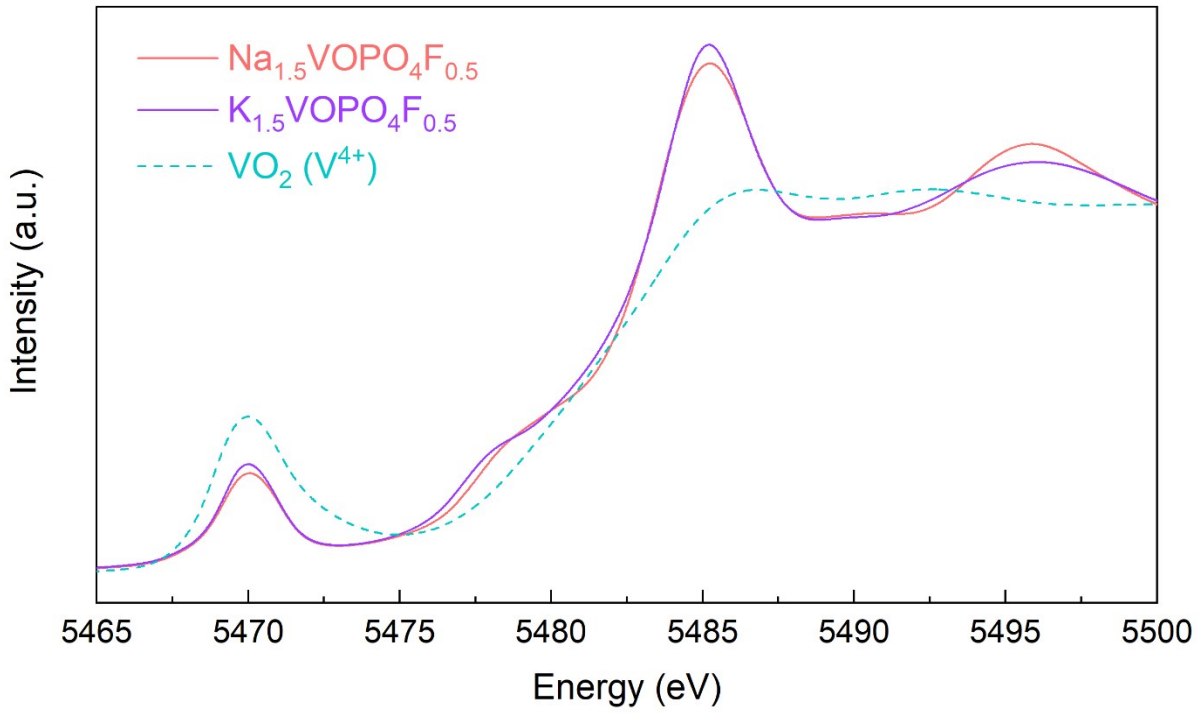

Fig. S16 V K-edge XANES spectrum of $Na_{1.5}VOPO_4F_{0.5}$ and $K_{1.5}VOPO_4F_{0.5}$.

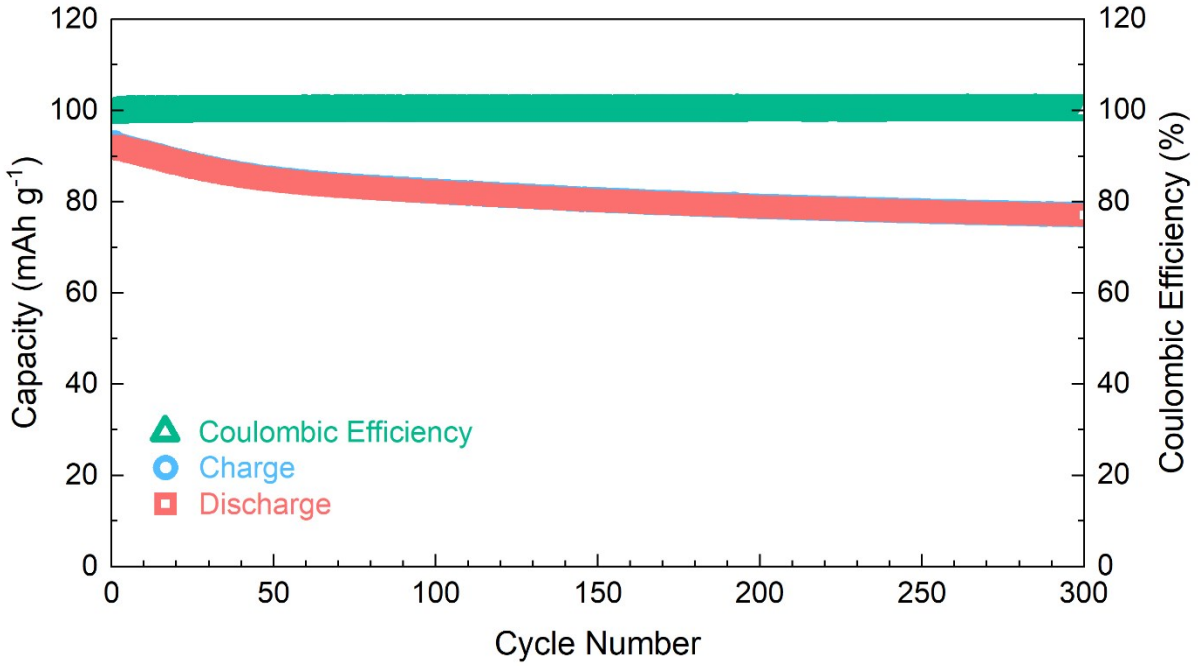

Fig. S17 Cycling performance of $K_{1.5}VOPO_4F_{0.5}$//hard carbon full-cell in the range of 1.7–4.4 V at 116 mA g^{-1} over 300 cycles.

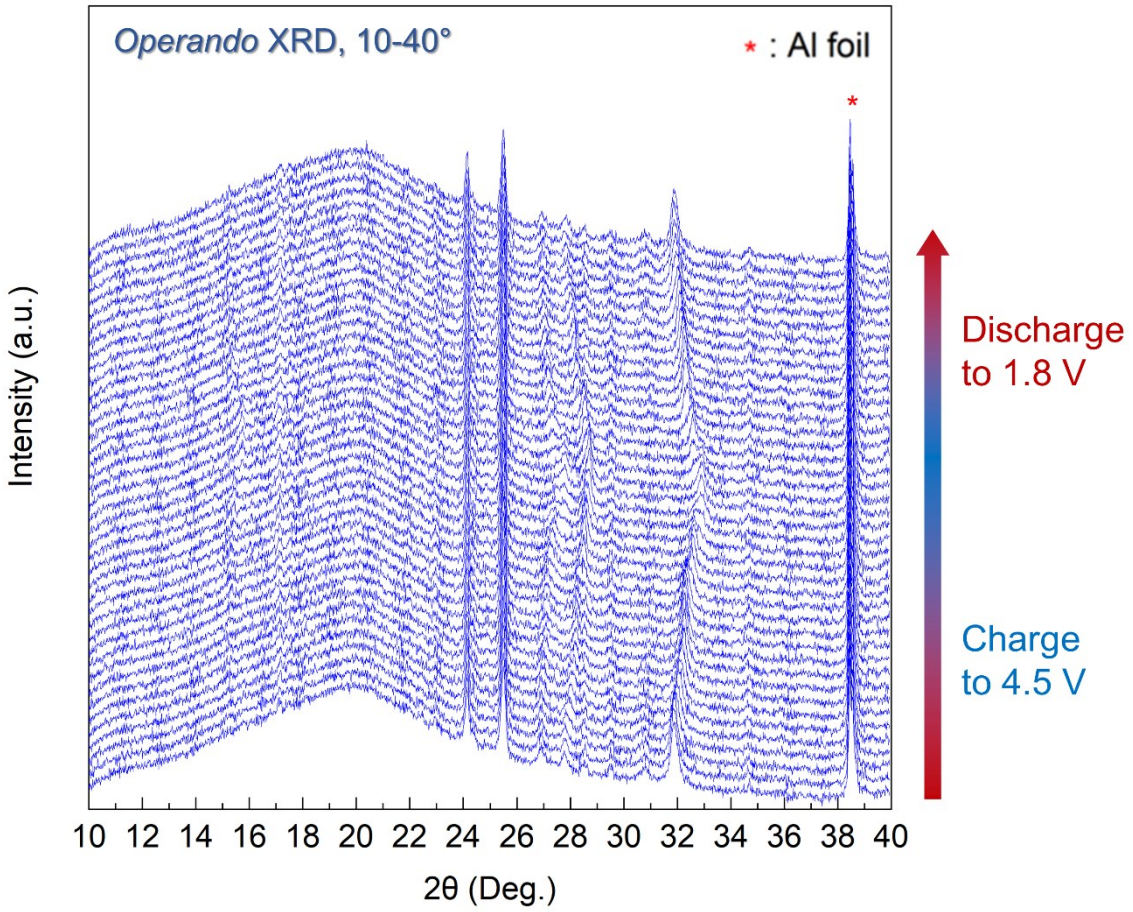

Fig. S18 Full *operando* XRD patterns of $K_xVOPO_4F_{0.5}$ ($0.5 \leq x \leq 1.5$).

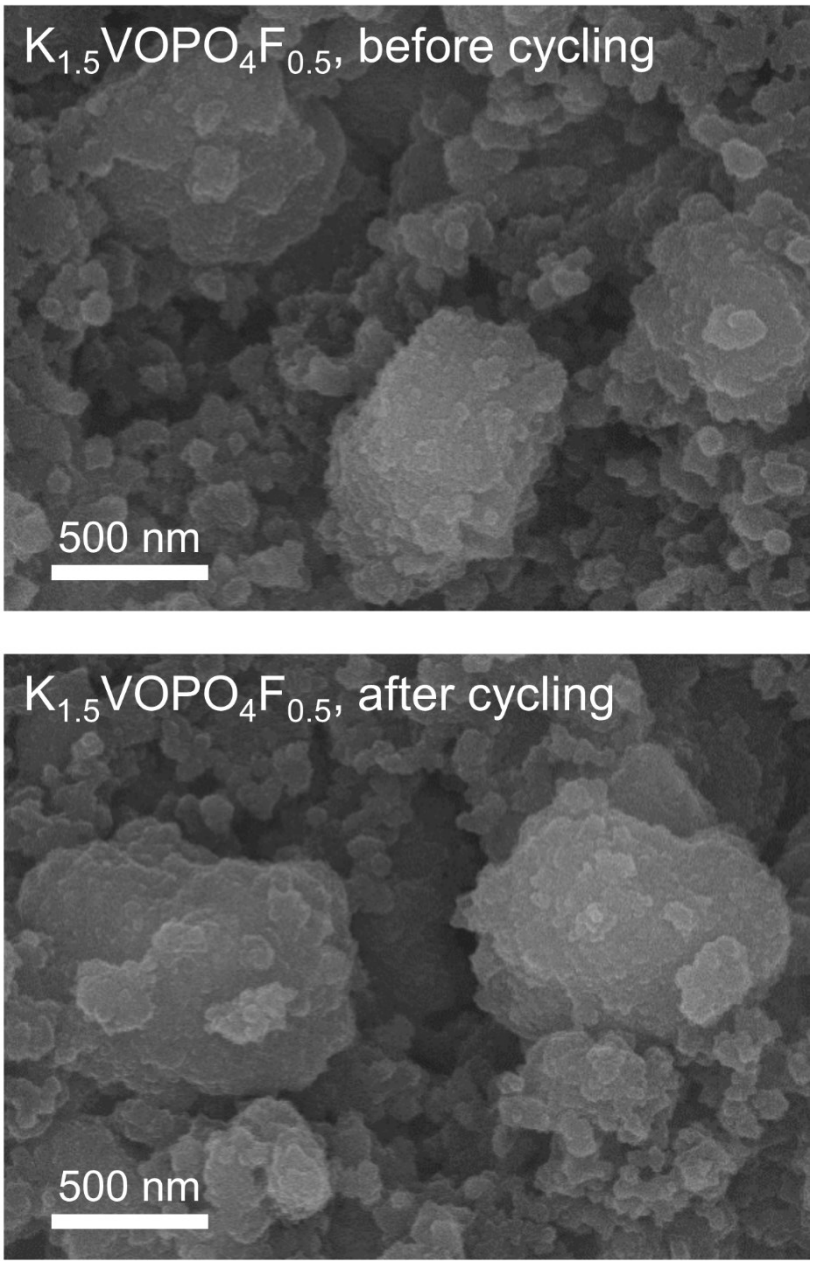

Fig. S19 SEM images of $K_{1.5}VOPO_4F_{0.5}$ before and after cycling.

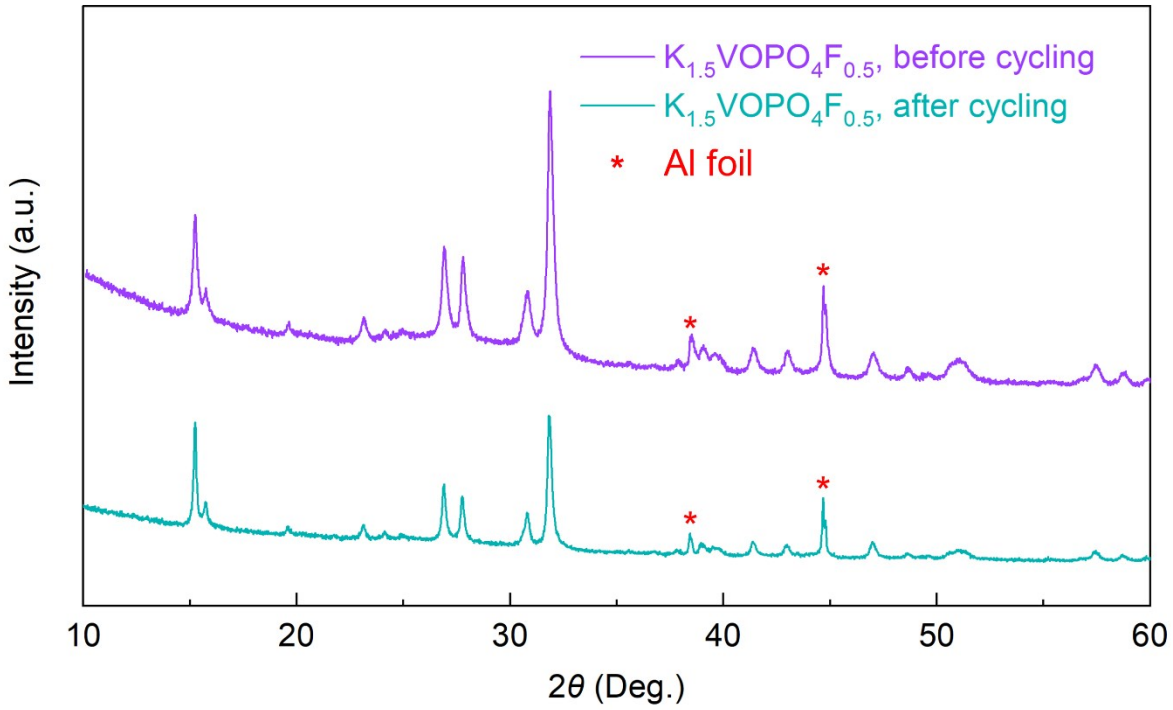

Fig. S20 XRD patterns of $K_{1.5}VOPO_4F_{0.5}$ before and after cycling.

Supplementary table

	Na	K	V	P
Re-obtained $Na_{1.5}VOPO_4F_{0.5}$	1.494	0	1.000	1.008

Table S1 ICP results of re-obtained $Na_{1.5}VOPO_4F_{0.5}$.

Cut-off voltage	Na	K	V	P
4.3 V	0.308	1.208	1.000	1.003
4.4 V	0.124	1.375	1.000	1.010
4.5 V	0	1.505	1.000	1.004

Table S2 ICP results of $K_{1.5}VOPO_4F_{0.5}$ with different cut-off voltage.

Crystal structure : Tetragonal

Space Group : $P\,4_2/m\,n\,m$

Lattice parameters : $a = b = 9.01024(9)$, $c = 10.6065(2)$

Atom	Wyckoff position	*x*	*y*	z	B_{iso}	Occupancy
V1	8j	0.2480(7)	0.2480(7)	0.20079(17)	1.09(4)	1
P1	4e	0	0	0.2441(17)	0.61(7)	1
P2	4d	0	0.5	0.25	0.61(7)	1
O1	8j	0.2510(18)	0.2510(18)	0.3557(4)	0.57(6)	1
O2	8j	0.0923(12)	0.0923(12)	0.161(2)	0.57(6)	1
O3	8j	0.4040(13)	0.4040(13)	0.161(3)	0.57(6)	1
O4	16k	0.0971(13)	0.4029(12)	0.1722(9)	0.57(6)	1
F1	4f	0.2523(17)	0.2523(17)	0	0.65(17)	1
Na1	8i	0.3070(10)	0.5346(16)	0	1.73(10)	0.7
Na2	8i	0.0107(12)	0.7395(17)	0	1.73(10)	0.8

Table S3 Detailed structural information of $Na_{1.5}VOPO_4F_{0.5}$.

Sample	*a* (Å)	*c* (Å)
$Na_{1.5}VOPO_4F_{0.5}$	9.01024(9)	10.6065(2)
$K_{1.5}VOPO_4F_{0.5}$	9.0633(2)	11.5776(6)

Table S4 Comparison of lattice parameters between $Na_{1.5}VOPO_4F_{0.5}$ and $K_{1.5}VOPO_4F_{0.5}$.

Crystal structure : Tetragonal

Space Group : $P\,4_2/m\,n\,m$

Lattice parameters : $a = b = 9.0633(2)$, $c = 11.5776(6)$

Atom	Wyckoff position	*x*	*y*	z	B_{iso}	Occupancy
V1	8j	0.2505(4)	0.2505(4)	0.1998(2)	0.68(6)	1
P1	4e	0	0	0.2328(10)	2.26(14)	1
P2	4d	0	0.5	0.25	2.26(14)	1
O1	8j	0.2473(11)	0.2473(11)	0.3310(6)	0.84(12)	1
O2	8j	0.0962(8)	0.0962(8)	0.1624(8)	0.84(12)	1
O3	8j	0.4029(8)	0.4029(8)	0.1795(9)	0.84(12)	1
O4	16k	0.1063(10)	0.4058(9)	0.1812(5)	0.84(12)	1
F1	4f	0.2338(11)	0.2338(11)	0	1.0(4)	1
K1	8i	0.3327(6)	0.5580(7)	0	0.96(9)	0.7
K2	8i	0.0315(6)	0.7161(7)	0	0.96(9)	0.8

Table S5 Detailed structural information of $K_{1.5}VOPO_4F_{0.5}$.

References

1 L. Tang, X. Liu, Z. Li, X. Pu, J. Zhang, Q. Xu, H. Liu, Y. G. Wang and Y. Xia, *ACS Appl. Mater. Interfaces*, 2019, **11**, 27813–27822.

2 X. Cao, X. Ren, L. Zou, M. H. Engelhard, W. Huang, H. Wang, B. E. Matthews, H. Lee, C. Niu, B. W. Arey, Y. Cui, C. Wang, J. Xiao, J. Liu, W. Xu and J.-G. Zhang, *Nat. Energy*, 2019, **4**, 796–805.

3 M. Hekmatfar, I. Hasa, R. Eghbal, D. V. Carvalho, A. Moretti and S. Passerini, *Adv. Mater. Interfaces*, 2020, **7**, 1901500.

4 R. R. Gaddam, E. Jiang, N. Amiralian, P. K. Annamalai, D. J. Martin, N. A. Kumar and X. S. Zhao, *Sustain. Energy Fuels*, 2017, **1**, 1090–1097.